

Dielectric and energy storage properties of barium strontium titanate based glass–ceramics prepared by sol–gel method

Qingyuan Hu · Tong Wang · Li Jin ·
Xiaoyong Wei

Received: 17 February 2014 / Accepted: 13 May 2014 / Published online: 25 May 2014
© Springer Science+Business Media New York 2014

Abstract Ba_{0.6}Sr_{0.4}TiO₃ based glass–ceramics were prepared by sol–gel process. Influences of B–Si–O glass content on the microstructure, dielectric, and energy storage properties of the BST based glass–ceramics have been investigated. Perovskite barium strontium titanate phase was found at annealing temperature 800 °C. A secondary phase Ba₂TiSi₂O₈ was detected and lowered by declining the mole ratio of element Si (from 50 to 25 mol%) in glass additive. Microstructural observation indicated that the microstructure homogeneity can be improved by glass addition till 2 mol%, while worsened by excessive glass concentrations. Due to relatively homogeneous microstructure, the maximum discharged energy density and breakdown strength were also obtained in samples with 2 mol% glass additive, which were found to be 0.553 J/cm³ and 43.2 kv/mm, respectively. Microscopic observation of the breakdown area was performed and the mechanical failure, including the formation and accumulation of micro-cracks during the dielectric breakdown process, was considered to be the main cause of dielectric breakdown. Results of the charging and discharging energy densities show that the BST based glass–ceramics prepared by sol–gel method has a potential for pulse power applications.

Keywords BST · Sol–gel · Glass–ceramics · Dielectric breakdown · Energy storage

1 Introduction

In recent years, because of the increasingly deteriorated energy crisis, more and more interests have been attracted on high energy storage devices. A variety of materials have been explored as dielectrics for energy storage capacitors, such as ceramics [1–4], glass–ceramics [5–8], and polymers [9]. In general, energy density is proportional with dielectric constant and dielectric breakdown strength square ($J = \frac{1}{2} \epsilon E_b^2$). By adjusting glass composition, glass–ceramics can achieve a compromised state where relative high permittivity and high breakdown strength coexist, which makes it a promising candidate for energy storage applications. Therefore, glass–ceramics attracted extraordinary attention among those materials.

Barium strontium titanate, Ba_{1-x}Sr_xTiO₃, is being widely investigated as a suitable dielectric material for high energy storage applications because of its high dielectric constant, low dielectric loss [10]. Many different methods of manufacturing BST glass–ceramics have been used. Melt-casting followed by controlled crystallization is a widely used one. In this approach, a glass matrix comprised of glass network formers and ferroelectric constituents is prepared by melt-casting. And then, the controlled crystallization takes place during the subsequent heat treatment. Zhang et al. successfully fabricated the BST ferroelectric glass–ceramics using BaO–SrO–TiO₂–Al₂O₃–SiO₂ system by the melt-casting and crystallization route. It was found that the maximum discharged energy storage density was 1.8 J/cm³ and the low released energy density

Q. Hu · T. Wang · L. Jin · X. Wei (✉)
Electronic Materials Research Laboratory, Key Laboratory of
the Ministry of Education, Xi'an Jiaotong University,
Xi'an 710049, China
e-mail: wdy@mail.xjtu.edu.cn

Q. Hu
e-mail: huqingyuan@stu.xjtu.edu.cn

Q. Hu · T. Wang · L. Jin · X. Wei
International Center for Dielectric Research, Xi'an Jiaotong
University, Xi'an 710049, China

in glass–ceramics was mainly caused by interfacial polarization [11]. More recently, Xiangrong Wang et al. [12] added AlF_3 into $\text{BaO–SrO–TiO}_2\text{–Al}_2\text{O}_3\text{–SiO}_2$ system and investigated effects of AlF_3 concentration on the microstructure and energy storage properties of BST glass–ceramics. The AlF_3 concentration dependence of energy storage properties revealed that both the charged and discharged energy densities increased with the increasing AlF_3 concentration (1–2 mol%) and then decreased at higher AlF_3 concentrations. Huang et al. [13] studied the correlation between the dielectric breakdown performance and interface polarization (also in BST glass–ceramics). According to the measurements of impedance spectroscopy as a function of sintering temperatures, it was found that the interface polarization critically lowered the breakdown performance. Although the BST ferroelectric glass–ceramics reported have both high dielectric constant and high dielectric breakdown strength, large unreleased-energy storage density caused by interfacial is a problem that needs to be addressed urgently.

Another way to prepare ferroelectric glass–ceramics is the sol–gel method. In previous studies, Zhang et al. [14] successfully prepared $\text{Ba}_3\text{Zn}_z\text{Co}_{2-z}\text{Fe}_{24}\text{O}_{41}/\text{SiO}_2$ glass ceramics via sol–gel method and the microwave properties were investigated. Crystallization and properties of sol–gel derived ferromagnetic glass ceramics were also reported in works by Zhai et al. [15]. Advantages of using sol–gel method include good capability in adjusting microstructures and the much lower operating temperature. Wu et al. [16, 17] prepared BST glass–ceramics by sol–gel method at a low sintering temperature. And the relationships between sintering conditions, microstructure, and dielectric properties were also reported. Hu et al. [18] also prepared BST glass–ceramics with B_2O_3 additive used as a microwave material. However, to date, few energy storage properties of the sol–gel prepared BST glass–ceramics was reported.

Recently, the present authors proposed a reverse boundary layer capacitor (RBLC) model in glass ceramic composites [19]. In the RBLC model, the grain boundary has a higher electrical conductivity than the grain, resulting in a larger electric field across grains and correspondingly smaller electric field across grain boundaries. The breakdown field is significantly improved because of the field distribution. The brick wall microstructure model is the premise of the RBLC theory. The well coated microstructure observed in this paper is exactly similar to the brick wall model. Therefore, glass–ceramics prepared by sol–gel method may provide experimental applications of the RBLC theory and achieve larger energy storage density by introducing glass additives with higher electrical conductivity.

The main purpose of the present work is to investigate the energy storage properties of BST glass–ceramics

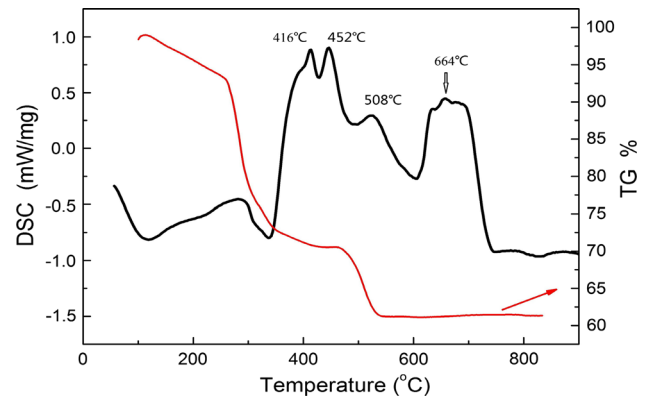


Fig. 1 DSC and TG curves of BST samples

prepared by sol–gel method. The base composition is $\text{Ba}_{0.6}\text{Sr}_{0.4}\text{TiO}_3$. At this Ba/Sr ratio, slim P–E loops with high polarization value and relatively small hysteresis loss were obtained, resulting in a large energy storage density. Microstructures and dielectric properties results were also reported in this paper.

2 Experimental procedures

Starting materials used for preparing (1– x) mol% $\text{Ba}_{0.6}\text{Sr}_{0.4}\text{TiO}_3$ –(x) mol% B–Si–O glass–ceramics were barium acetate ($\text{Ba}(\text{AC})_2$), strontium acetate hemihydrate ($\text{Sr}(\text{AC})_2 \cdot 1/2\text{H}_2\text{O}$), titanium isopropoxide ($\text{Ti}(\text{OCH}(\text{CH}_3)_2)_4$), tributyl borate ($\text{B}(\text{OCH}_2\text{CH}_2\text{CH}_2\text{CH}_3)_3$), tetraethyl orthosilicate ($(\text{C}_2\text{H}_5\text{O})_4\text{Si}$), acetic acid (HAC). The glass composition was set as 75 % B–25 % Si (mol%). And the proportion of glass additive was 0 mol% (BST), 2 mol% (BST-G02), 5 mol% (BST-G05), 10 mol% (BST-G10), respectively. These starting materials were used according to the stoichiometry of each component. Sol–gel experiment routes are shown in Fig. 1.

Firstly, barium acetate (99.0 %) and strontium acetate (99.0 %) were dissolved in acetic acid (99.0 %) in sequence. Titanium isopropoxide was dissolved in Ethanol with acetic acid as the stabilizer and catalyzer. Then, the above mixture was slowly dropped into the Ba–Sr solution. Meanwhile, tributyl borate and tetraethyl orthosilicate were mixed with alcohol, acetic acid and deionized water, followed by stirring for 1 h. And subsequently, the Ba–Sr–Ti–O precursor and B–Si–O precursor were intensively mixed. After hydrolysis polymerization reaction, a transparent and clear Ba–Sr–Ti–B–Si–O sol was formed and finally turned into gel. The gel was heat treated first at 80 °C (4 h) and after at 200 °C (4 h). Powder samples were obtained after annealing at 800 °C. The powders were mixed with PVA, and then pressed into pellets of 12 mm in diameter. After

Table 1 Compositions of BST samples

Sequence number	Glass component	Composition (mol%)
BST	/	Ba _{0.6} Sr _{0.4} TiO ₃
BSTG-02	0.75B-0.25Si(G1)	0.98(Ba _{0.6} Sr _{0.4} TiO ₃)-0.02(G1)
BSTG-05	0.75B-0.25Si(G1)	0.95(Ba _{0.6} Sr _{0.4} TiO ₃)-0.05(G1)
BSTG-10-1	0.75B-0.25Si(G1)	0.9(Ba _{0.6} Sr _{0.4} TiO ₃)-0.1(G1)
BSTG-10-2	0.5B-0.5Si(G2)	0.9(Ba _{0.6} Sr _{0.4} TiO ₃)-0.1(G2)

de-blending, these pellets were sintered at temperatures from 1,200 to 1,300 °C in air. Compositions of different samples are given in Table 1.

Dry gel powders were analyzed by thermo-gravimetric analysis (TG) and differential scanning calorimeter (DSC) (Thermal analyzer: STA449C, NETZSCH). Phase structure of the samples was studied by a X-ray diffractometer (XRD) (Model D/Max-IIIC, Rigaku, Tokyo, Japan, Cu K α , $\lambda = 1.54178 \text{ \AA}$). Scanning electron microscopy (SEM) and energy disperse spectroscopy (EDS) were performed in (FEI quantum FEG250) to investigate microstructures. And the dielectric temperature spectra were measured by a LCR meter (HP 4284, Agilent, Palo Alto, CA) with a frequency range from 1 kHz to 1 MHz. Ferroelectric hysteresis loops (P–E) were measured by a modified Sawyer–Tower circuit. All P–E curves were measured at room temperature and a low frequency of 1 Hz. Electric fields were supplied by a high voltage power supply (Trek 609-B, NY, USA) which was driven by a frequency generator (HP 33220A, CA, USA). Samples used for P–E measurements were processed into disks (10 mm in diameter and about 0.25 mm in thickness). And then, these samples were covered with gold electrodes after polishing. Polarizing microscope (OLYMPUS BX51 M) was used for Optical observation. Dielectric breakdown strength measurement was performed on a CJ2671 high voltage tester under the DC condition. Samples used for dielectric breakdown measurement were without electrodes.

3 Results and discussion

Thermal analysis results of the BST glass–ceramics gel with a heating rate of 10 °C/min are shown in Fig. 1. Associated with XRD patterns shown in Fig. 2, the crystallization process can be elaborated. In DTA/TG curves, notable weight loss below 600 °C is attributed to evaporation of the solvent. According to XRD patterns shown in Fig. 2 (curve d), only small amounts of BaCO₃ phase

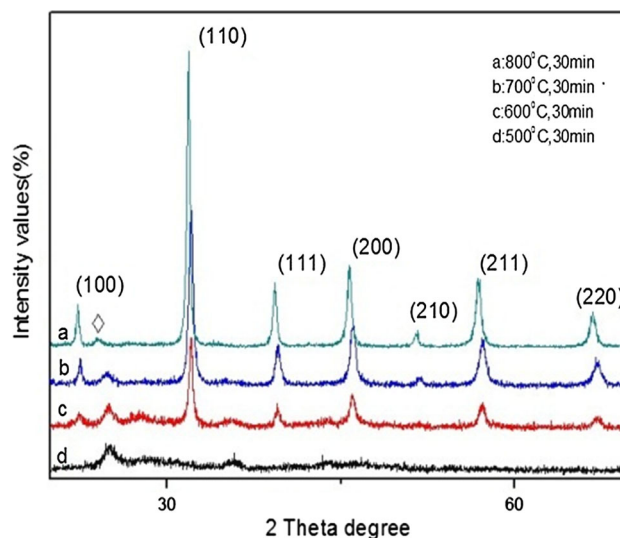


Fig. 2 XRD patterns of pure BST glass–gels heat treated at different temperatures (diamond BaCO₃)

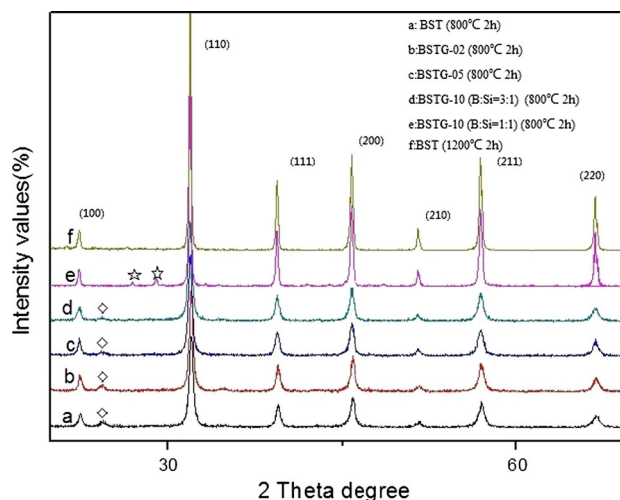
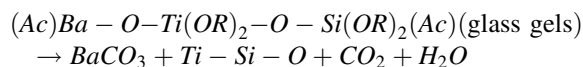


Fig. 3 XRD patterns of different BST based glass–ceramic samples (star Ba₂TiSi₂O₈; diamond BaCO₃)

crystallization appears under 600 °C. The crystallization reaction process of BaCO₃ phase may be described as:



Exothermic peaks below 600 °C are caused by decomposition and burning of the organic radicals. At 664 °C, an exothermic peak occurs without any weight loss. Combined with XRD patterns (curve b c), it is found that this exothermic peak means the crystallization of BST phase. Figure 3 shows the XRD patterns of the glass–ceramic specimens. Structural phase of cubic perovskite is formed

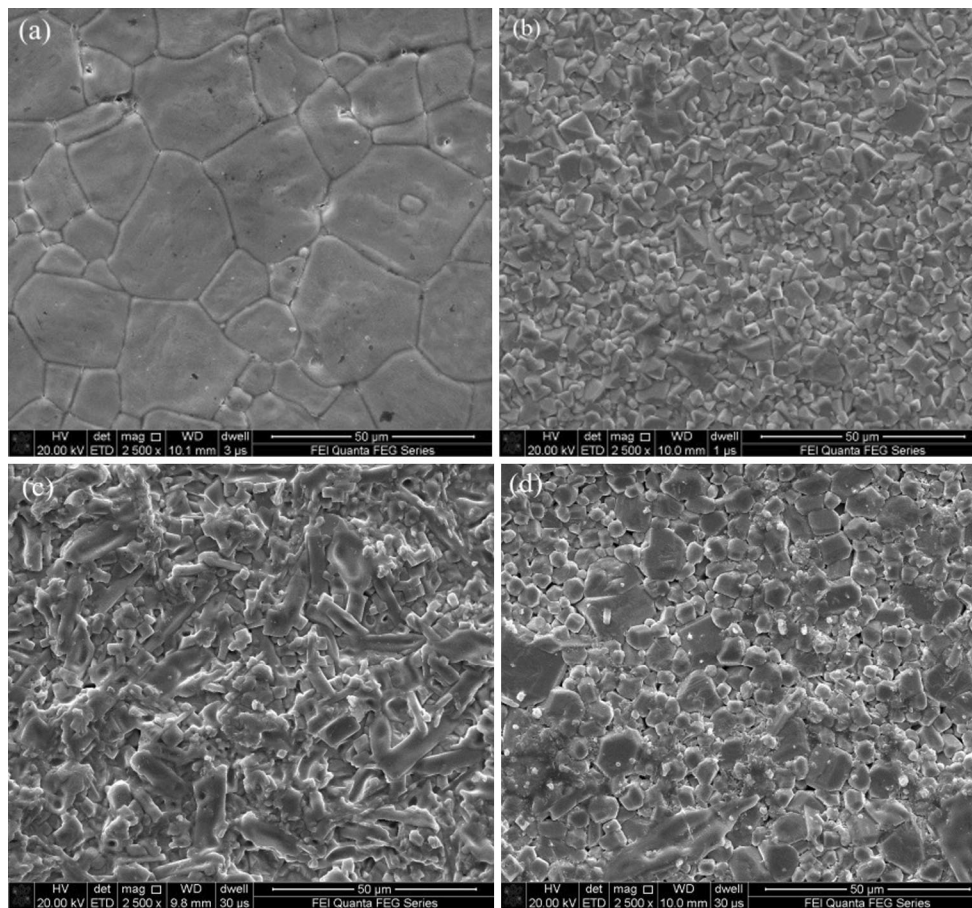
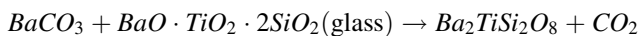


Fig. 4 SEM images of the natural surface of **a** BST 2500*, **b** BSTG-02 2500*, **c** BSTG-05 2500*, **d** BSTG-10 2500*

as the major phase at annealing temperature 800 °C (PDF#34-0411). A small amount of $(\text{Ba,Sr})\text{CO}_3$ phase is also detected at 800 °C (curve a). And then this $(\text{Ba,Sr})\text{CO}_3$ phase decomposed at higher annealing temperature 1,200 °C (curve f). In specimens with G1 additive, no remarkable secondary phase was detected (curve b c d). However, a phase of $\text{Ba}_2\text{TiSi}_2\text{O}_8$ appeared in specimens with G2 additive (curve e). The chemical reaction equation of $\text{Ba}_2\text{TiSi}_2\text{O}_8$ crystallization is that:



The impurity phase is attributed to the reaction between glass additive with higher [Si] content and the BST phase.

Scanning electron micrographs of BST glass–ceramics with different amounts of glass additive were shown in Fig. 4. Pure BST samples have highly inhomogeneous microstructure, which shows very large grains coexist with very small ones. It can be seen that the average grain size decreased significantly with 2 mol% glass concentrations. Figure 5 shows a more detailed observation of BSTG-02 samples. Some thin layer materials are found on the surroundings of grains. EDS analysis of grains and grain

boundaries is also shown in Fig. 5. Only a corresponding proportion of BST elements are detected in 1# area (grain). However, except for BST phase elements, glass additive elements ([B] [Si]) are also found in 2# area (grain boundary). So, it can be concluded that these thin layer materials are glass additives and BST grains are coated by glass additive layers. This coated structure is understood to occur because BST grains are crystallized from glass matrix and embedded in glass phase. During sintering process, grains grow larger and larger. At the same time, the glass phase is distributed at the surroundings of grains uniformly. And then, the well coated structure is formed. Porosity is also suppressed by this microstructure. However, as the glass content increased to 5 mol%, this well coated microstructure is broken. It is found that the glass phase sticks together and is separated from the ceramic phase. This phenomenon became more evident in 10 mol% glass-added BST glass ceramic samples shown in Fig. 4d. The microstructure transformation might be caused by agglomeration of glass additives which happens at excessive glass concentrations. Thus, it can be concluded that proper glass additive can decrease grain size and form the coated structure. But excessive glass concentration will

Fig. 5 EDS analysis of the grain (1#) and grain boundary (2#) of BSTG-02 samples

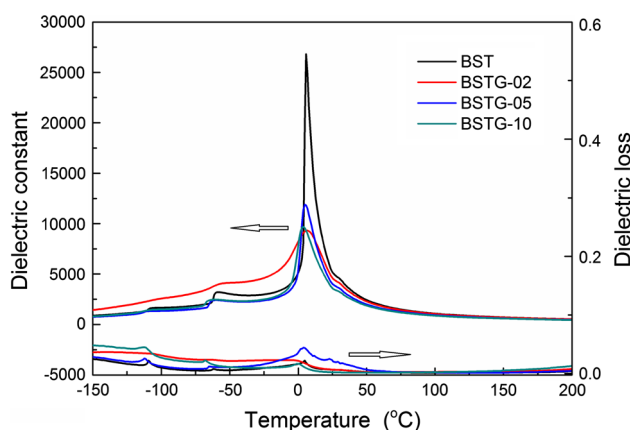
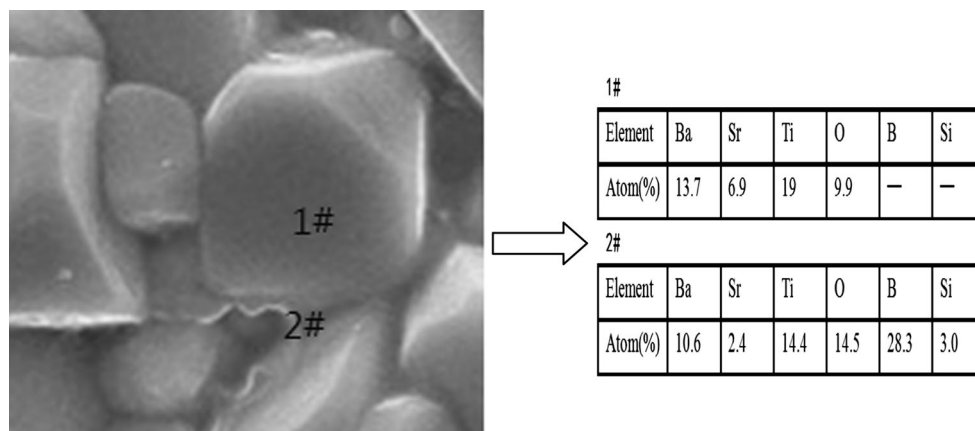


Fig. 6 Temperature dependence of dielectric constant and dielectric loss of samples with different glass concentrations at 10 kHz

destroy the homogeneous microstructure. Similar results were also reported by J W Zhai et al. In Zhai's work, samples with 2 wt% AZO glass content have more homogenous and dense microstructure than samples with more AZO glass content [20].

Effects of glass concentration on the temperature-dependent dielectric properties of the BST glass-ceramics in the temperature range of -150 to 200 °C is illustrated in Fig. 6. The maximum dielectric constant decreases as the glass phase was added. This is due to the impurity phase and the significantly reduced grain size caused by glass additives. It is obtained that plots of the dielectric constant versus temperature of pure BST samples has three peaks, which situates at about -110 , -65 and 10 °C respectively. And each peak corresponds to a structural phase transition with increasing temperature. From low to high temperature, the structural phase transition is Rhombohedral/Octahedral/Tetragonal/Cubic, in turn [21]. All the peak values at the three temperature regimes increase as glass content decreases, except for BSTG-02 samples.

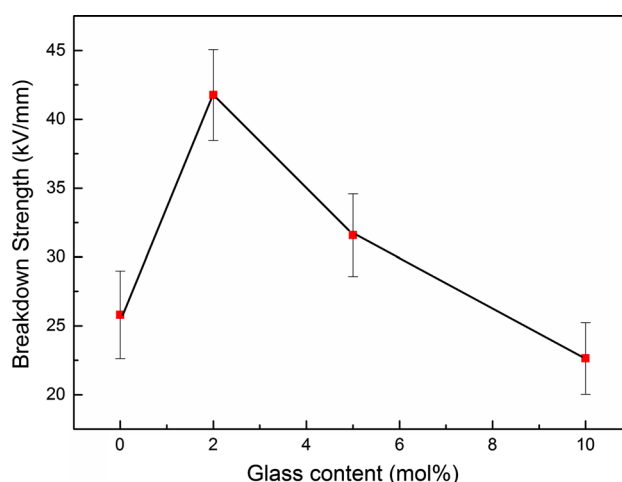


Fig. 7 The average breakdown strength of the BST based glass-ceramics as a function of glass additive

Meanwhile, T_{max} , at which the maximum permittivity was observed, decreased slightly with the increase of glass additives. Temperature dependence of dielectric loss is also shown in Fig. 6.

Figure 7 shows the average breakdown strength of the BST based glass-ceramics as a function of glass additive. The average breakdown strength increases firstly, getting its maximum value at 2 mol% glass concentration, and then decreases with the increasing glass content. Pure BST samples have the average breakdown strength of 27.5 kV/mm. The highest average breakdown strength value is obtained from 2 mol% glass-added samples, which is found to be 43.2 kV/mm. Then, as glass content increases from 2 to 10 mol%, the average breakdown strength drops from 43.2 to 21.4 kV/mm. This variation of the average breakdown strength is closely related to the microstructures. It is well known that the dielectric breakdown strength of glass-ceramics is mainly influenced by porosity [22], grain size [23] and interfacial polarization [13]. Low

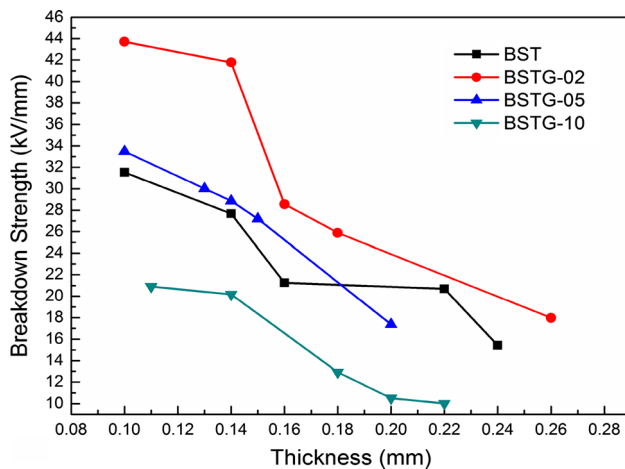


Fig. 8 Thickness dependence of breakdown strength of samples with different glass concentrations

porosity, fine grain and less interfacial polarization are beneficial to obtain high dielectric breakdown strength. BSTG-02 sample has the most homogeneous microstructure and the grain size is also smaller than other samples. In the microstructure of BSTG-02 samples, the glass phase is uniformly distributed at grain boundaries. Interfacial polarization and porosity can be drastically reduced by the coated structure. Consequently, BSTG-02 samples have the maximum average breakdown strength. As glass content continues to increase, the coated structure is broken. Porosity increases and more interfacial polarization appear. This variation leads to a significant drop of the dielectric breakdown strength. Dielectric strength of BST glass-ceramic samples versus thickness is plotted in Fig. 8. In all curves, it is found that dielectric strength generally decreases as the increasing thickness. It is a reasonable result because there are less defects existing in samples with lower thickness values.

The broken samples were inspected by optical microscope to study the breakdown process from the aspect of mechanical failure. It can be seen from Fig. 9 that a breakdown channel passes through the sample and is ended by a ‘crater’ at the surface of the sample [24]. The breakdown channel is found to be initially formed at the weak regions inside the sample. Pores and defects located in the weak regions would result in local field concentration leading to a rise in local temperature because of Joule heating effect. The induced temperature gradient between weak regions and the surrounding regions may produce mechanical stress, and therefore, form micro-cracks. As the electric field increases, the micro-cracks grow larger and larger. By connecting with each other, the breakdown channel is formed finally. Molten matter expelled from the dielectric breakdown channel can be observed around the

crater. This can be used as a direct evidence of the temperature gradient and local heating. Dielectric breakdown emerges through the breakdown channel which can be regarded as an electrical conduction path [25].

P–E hysteresis loop measurements were performed on the BST based glass-ceramics fabricated in this study to examine their energy storage properties. Effects of glass concentration on the P–E hysteresis loops for the BST based glass-ceramics are shown in Fig. 10. Each of these loops was measured up to their breakdown field (E_b). It can be seen that the maximum polarization value is obtained in samples with 2 mol% glass concentrations, due to its high max electric field. The maximum E_b value, 12 kv/mm, is also found in 2 mol% glass additive samples. And then, as glass content increases, the E_b values gradually decrease to 7.8 kv/mm for 10 mol% glass additive. In addition, with 2 mol% glass concentration, the hysteresis loop is slimmer than other loops. Unfortunately, all these max electric fields are far from their average breakdown strength. This may due to the different methods of testing and effects of electrode area. The average breakdown strength was measured under DC voltage and without electrodes. Moreover, compared to surface contact in P–E measurements, point contact was used in average breakdown strength tests. Hence, the breakdown probability is larger in P–E measurements.

Variation in E_{max} values revealed that appropriate glass concentration could enhance the breakdown strength. However, interfacial polarization and porosity caused by excessive glass additive deteriorated the breakdown strength. Moreover, glass additive could also reduce the polarization value. Therefore, to obtain the optimal energy storage density, the glass content should be controlled in a relatively lower range.

The charged energy density is equal to the integral of the area enclosed by charge curve and y-axis. The discharged energy density is equal to integral of the area enclosed by discharge curve and y-axis. The unreleased energy density or the energy loss is equal to integral of the area enclosed by charge and discharge curve and y-axis. The ratio of discharged and charged energy density can be used to evaluate the energy efficiency. The charged/discharged energy densities and energy efficiency of the BST based glass-ceramics were shown in Table 2. It is found that all the values have the same variation as the average breakdown strength. The maximum discharged energy density of 0.553 J/cm^3 and the highest energy efficiency of 94.5 % are obtained in samples with 2 mol% glass additive. From Fig. 4, the microstructures of BST glass-ceramics prepared by sol-gel method have strong impacts on their energy storage properties. Samples with 2 mol% glass concentration have the most homogeneous and glass coated microstructure. Excessive glass additive may destroy the

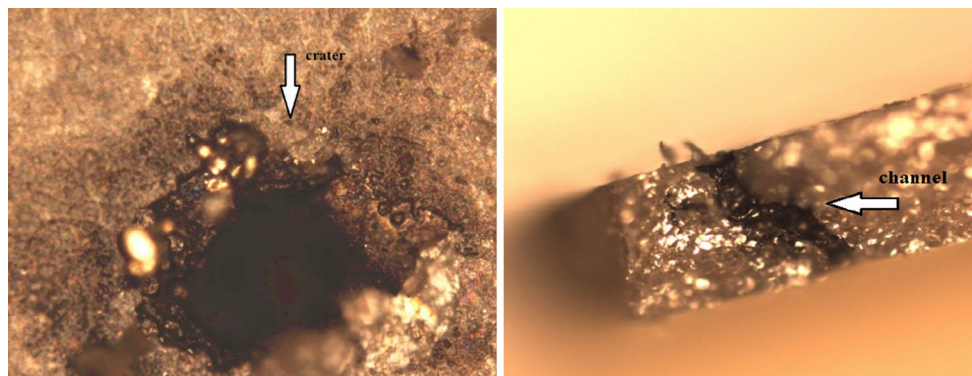


Fig. 9 Optical observation of the broken samples

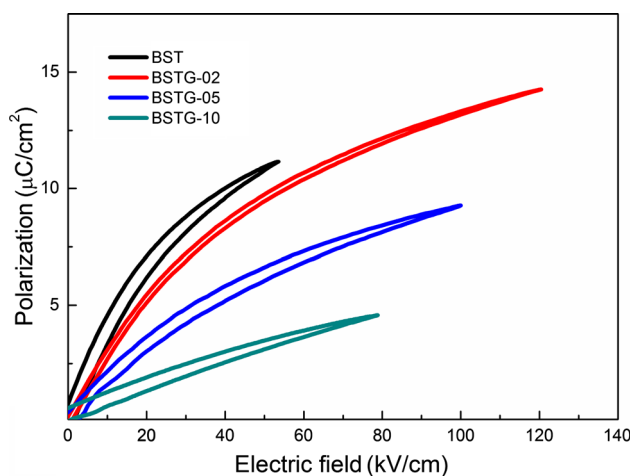


Fig. 10 P–E loops of BST samples with different glass concentrations

Table 2 The charged/discharged energy densities and energy efficiency of the BST based glass–ceramic samples

Sequence number	Charged energy density (J/cm^3)	Discharged energy density (J/cm^3)	Energy efficiency (%)
BST	0.233	0.192	82.4
BSTG-02	0.585	0.553	94.5
BSTG-05	0.369	0.321	86.9
BSTG-10	0.169	0.136	80.5

microstructure and worsen the related energy storage properties.

4 Conclusion

The BST based glass–ceramics with different glass concentrations were successfully fabricated by sol–gel method.

It is shown in XRD patterns and DTA/TG curves that the perovskite BST phase is crystallized from the glass–gel. The SEM images indicate that a well-coated and uniform microstructure was obtained in samples with 2 mol% glass concentration. The highest average breakdown value of 43.2 kV/mm and the maximum discharged energy density of 0.553 J/cm^3 was also measured in these samples because of the well coated microstructure. Observations of the broken samples show a breakdown channel inside the sample. It can be inferred that the breakdown strength will be increased by reducing the porosity and defects.

Acknowledgments This work is supported by the International Science and Technology Cooperation Program of China (2013DFR50470) and “111” Project (B14040).

References

- Burn I, Smyth DM (1972) *J Mater Sci* 7:339–343
- Gao F, Dong XL, Mao CL, Liu W (2011) *J Am Ceram Soc* 94:4382–4386
- Shay DP, Podraza NJ, Donnelly NJ, Randall CA (2012) *J Am Ceram Soc* 95:1348–1355
- Ogihara H, Randall CA, Susan TM (2009) *J Am Ceram Soc* 92:1719–1724
- Gorzowski EP, Pan MJ, Bender B, Wu CCM (2007) *J Electroceram* 18:269–276
- Luo J, Du J, Tang Q, Mao CH (2008) *IEEE Trans Electron Devices* 55:3549–3554
- Chen GH, Zhang WJ, Liu XY, Zhou CR (2011) *J Electroceram* 27:78–82
- Zhang QM, Wang L, Luo J, Tang Q (2009) *J Am Ceram Soc* 92:1871–1873
- Chu BJ, Zhou X, Ren KL, Zhang QM (2006) *Science* 21:334–336
- Fletcher NH, Hilton AD, Ricketts BW (1996) *J Phys D Appl Phys* 29:253–258
- Zhang Y, Huang JJ, Ma T, Wang XR (2011) *J Am Ceram Soc* 94:1805–1810
- Wang XR, Zhang Y, Ma T, Yuan ZB (2013) *Int J Appl Ceram Technol* 10:301–306
- JJ Huang, Y Zhang, T Ma, HT Li (2010) *Applied Physics Letters* 96:042902
- H Zhang, X Yao, L Zhang (2002) *Mater Res Innov* 5:117–122

15. Zhai JW, Yao X (2001) *Ferroelectrics* 262:25–30
16. Wu B, Zhang LY, Yao X (2004) *Ceram Int* 30:1757–1761
17. Wu B, Zhang LY, Yao X (2004) *Ceram Int* 30:1753–1756
18. Hu T, Jantunen H, Uusimaki A, Leppavuori S (2003) *Mater Sci Semicond Process* 5:215–221
19. Wei XY, Yan HX, Wang T, Hu QY (2013) *J Appl Phys* 113:024103
20. Xu C, Shen B, Zhai JW (2012) *Key Eng Mater* 512–515:1635–1640
21. Menoret C, Kiat JM, Dkhil B, Dunlop M (2002) *Phys Rev B* 65:224104
22. Wu ZH, Liu HX, Cao MH, Shen ZY (2008) *J Ceram Soc Jpn* 116:345–349
23. Tunkasiri T, Rujijanagul G (1996) *J Mater Sci Lett* 15:1767–1769
24. Owate IO, Freer R (1992) *J Appl Phys* 72:2418–2422
25. Malec D, Bley V, Talbi F (2010) *F Lalam* 30:3117–3123